Two phylogenetically and compartmentally distinct CDP-diacylglycerol synthases cooperate for lipid biogenesis in *Toxoplasma gondii*

Received for publication, October 31, 2016, and in revised form, March 17, 2017 Published, Papers in Press, March 17, 2017, DOI 10.1074/jbc.M116.765487

Pengfei Kong[‡], Christoph-Martin Ufermann[‡], Diana L. M. Zimmermann[‡], Qing Yin[§], Xun Suo[§], J. Bernd Helms[¶], Jos F. Brouwers[¶], and Nishith Gupta[‡1]

From the [‡]Department of Molecular Parasitology, Humboldt University, Berlin 10115, Germany, [§]National Animal Protozoa Laboratory and College of Veterinary Medicine, China Agricultural University, Beijing 100094, China, and [¶]Department of Biochemistry and Cell Biology, Institute of Biomembranes, Utrecht University, Utrecht 3584CM, Netherlands

Edited by George M. Carman

***Toxoplasma gondii* is among the most prevalent protozoan parasites, which infects a wide range of organisms, including one-third of the human population. Its rapid intracellular replication within a vacuole requires efficient synthesis of glycerophospholipids. Cytidine diphosphate-diacylglycerol (CDP-DAG) serves as a major precursor for phospholipid synthesis. Given the peculiarities of lipid biogenesis, understanding the mechanism and physiological importance of CDP-DAG synthesis is particularly relevant in *T. gondii*. Here, we report the occurrence of two phylogenetically divergent CDP-DAG synthase (CDS) enzymes in the parasite. The eukaryotic-type *Tg*CDS1 and the prokaryotic-type *Tg*CDS2 reside in the endoplasmic reticulum and apicoplast, respectively. Conditional knockdown of *Tg*CDS1 severely attenuated the parasite growth and resulted in a nearly complete loss of virulence in a mouse model. Moreover, mice infected with the *Tg*CDS1 mutant became fully resistant to challenge infection with a hyper-virulent strain of *T. gondii*. The residual growth of the *Tg*CDS1 mutant was abolished by consecutive deletion of *Tg*CDS2. Lipidomic analyses of the two mutants revealed significant and specific declines in phosphatidylinositol and phosphatidylglycerol levels upon repression of *Tg*CDS1 and after deletion of *Tg*CDS2, respectively. Our data suggest a "division of labor" model of lipid biogenesis in *T. gondii* in which two discrete CDP-DAG pools produced in the endoplasmic reticulum and apicoplast are subsequently used for the synthesis of phosphatidylinositol in the Golgi bodies and phosphatidylglycerol in the mitochondria. The essential and divergent nature of CDP-DAG synthesis in the parasite apicoplast offers a potential drug target to inhibit the asexual reproduction of *T. gondii*.**

Toxoplasma belongs to a group of unicellular parasites that comprises some of the most notorious pathogens of humans and animals, such as *Plasmodium*, *Cryptosporidium*, *Eimeria*, *Trypanosoma*, and *Leishmania*. One single species of *Toxoplasma*, *i.e. Toxoplasma gondii*, is able to infect and reproduce in most nucleated cells of virtually all warm-blood organisms. The widespread success of *T. gondii* depends on reversible switching of its two asexual stages known as tachyzoites and bradyzoites, which cause acute and chronic infection, respectively (1). Although infection is usually asymptomatic in healthy human adults, the acute infection of developing fetus and individuals with deteriorated immunity can be potentially fatal due to severe tissue necrosis caused by successive rounds of lytic cycles. The rapid intracellular replication of tachyzoites and concurrent expansion of the enclosing vacuole necessitate a significant membrane biogenesis.

The parasite membranes consist of polar and neutral lipids (2, 3). We have shown that glycerophospholipids account for a major fraction of total membrane lipids isolated from purified tachyzoites. Phosphatidylcholine (PtdCho)[2] is the most abundant glycerophospholipid present in tachyzoites followed by phosphatidylethanolamine (PtdEtn), phosphatidylthreonine (PtdThr), phosphatidylinositol (PtdIns), phosphatidylserine (PtdSer), phosphatidylglycerol (PtdGro), and phosphatidic acid (PtdOH) (2, 4). Our previous work has also identified the pathways of PtdCho, PtdEtn, PtdThr, and PtdSer synthesis in the parasite (4–7). Synthesis of PtdCho, PtdThr, and PtdSer occurs in the endoplasmic reticulum (ER), whereas PtdEtn can be made in the ER, mitochondrion, and parasitophorous vacuole. Endogenous production of glycerophospholipids begins with the synthesis of glycerol 3-phosphate and fatty acids from glucose-derived carbon (8–10). The parasite produces short acyl chains through a prokaryotic-type (type II) fatty acid synthase pathway located in the apicoplast (8), a non-photosynthetic

This work was supported by German Research Foundation (DFG) Grants GU1100/3-1 and GU1100/4-1 and a Heisenberg program award (to N. G.). The authors declare that they have no conflicts of interest with the contents of this article.
This article contains supplemental Tables S1 and S2 and Fig. S1.

[1] To whom correspondence should be addressed: Dept. of Molecular Parasitology, Humboldt University, Philippstrasse 13, House 14, Berlin 10115, Germany. Tel.: 49-30-20936404; Fax: 49-30-20936051; E-mail: Gupta.Nishith@staff.hu-berlin.de.

[2] The abbreviations used are: PtdCho, phosphatidylcholine; PtdEtn, phosphatidylethanolamine; PtdThr, phosphatidylthreonine; PtdIns, phosphatidylinositol; PtdSer, phosphatidylserine; PtdGro, phosphatidylglycerol; PtdOH, phosphatidic acid; ER, endoplasmic reticulum; DAG, diacylglycerol; CDP, cytidine diphosphate; CDS, CDP-DAG synthase; DHFR-TS, dihydrofolate reductase-thymidylate synthase; S.C., selection cassette; ATc, anhydrotetracycline; CAT, chloramphenicol acetyltransferase; HFF, human foreskin fibroblast; PIS, PtdIns synthase; PtdGro-P, PtdGro phosphate; PGPS, PtdGro-P synthase; m.o.i., multiplicity of infection; COS, crossover sequence; HXGPRT, hypoxanthine-xanthine-guanine phosphoribosyltransferase; *Tg*, *T. gondii*; gDNA, genomic DNA; UPRT, uracil phosphoribosyltransferase.

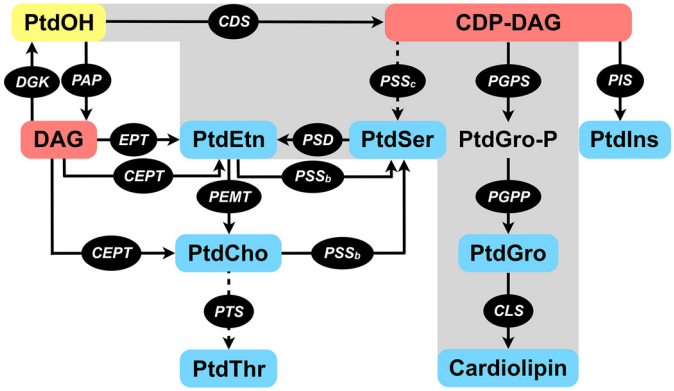

Figure 1. Synthesis of major phospholipids in eukaryotes and prokaryotes. Pathways shown in *solid arrows* correspond to mammalian cells (human/mouse) and/or eubacteria. All depicted pathways except for PSS_c and PTS (shown with *dotted arrows*) are present in mammalian cells, whereas bacteria harbor only the *gray-shaded* part of the network including PSS_c. A *bona fide* PTS has been recently identified in the apicomplexan parasite *T. gondii*. The end phospholipids are highlighted in *blue*; intermediates of synthesis are displayed in *red*, and underlying enzymes are in *black*. PtdOH (*yellow*) serves as the central precursor for the synthesis of all key phospholipids. *CDS*, CDP-DAG synthase; *CEPT*, choline/ethanolamine phosphotransferase; *CLS*, cardiolipin synthase; *DGK*, diacylglycerol kinase; *EPT*, ethanolamine phosphotransferase; *PAP*, phosphatidic acid phosphatase; *PEMT*, phosphatidylethanolamine *N*-methyltransferase; *PGPP*, phosphatidylglycerol phosphate phosphatase; *PGPS*, phosphatidylglycerol phosphate synthase; *PIS*, phosphatidylinositol synthase; *PSD*, phosphatidylserine decarboxylase; PSS_b, phosphatidylserine synthase (base-exchange type); PSS_c, phosphatidylserine synthase (CDP-DAG-dependent); *PTS*, phosphatidylthreonine synthase.

plastid-like organelle acquired by secondary endosymbiosis of red algae (11). These acyl chains can be exported to the ER, where they are modified to generate long-chain and unsaturated fatty acids (9).

Glycerol 3-phosphate and fatty acids are utilized to synthesize PtdOH. In mammalian cells, PtdOH is a central intermediate lipid that serves as the precursor to make other glycerophospholipids (12, 13). PtdOH is first converted to diacylglycerol (DAG) or CDP-DAG (Fig. 1). DAG enables the synthesis of PtdCho and PtdEtn, whereas CDP-DAG is utilized to make PtdIns and PtdGro. Prokaryotes lack the enzyme to produce DAG and deploy CDP-DAG as the progenitor for all glycerophospholipids (Fig. 1, *shaded*). The enzyme CDP-DAG synthase is, therefore, regarded as one of the most central enzymes of lipid synthesis in prokaryotes as well as in eukaryotes. Given the functional integration of apicoplast with other organelles harboring lipid synthesis, understanding the mechanism and relevance of CDP-DAG synthesis is particularly interesting in *T. gondii* but has not yet been studied. The parasite may also access host-derived CDP-DAG; it is unknown, however, whether tachyzoites can scavenge this lipid from the environment.

This work identified two phylogenetically distinct routes of CDP-DAG synthesis located in the ER and apicoplast of *T. gondii*, which have evolved to be primarily non-redundant and in fact functionally complementary to each other. We show that the two sources of CDP-DAG facilitate the synthesis of PtdIns and PtdGro, presumably in the Golgi complex and mitochondrion, respectively. The work suggests a substantial spatial segregation and inter-organelle trafficking of lipids. Metabolic autonomy of tachyzoites and evolutionary divergence of CDP-DAG pathway in the apicoplast also provide an opportunity to selectively inhibit the parasite development.

Results

T. gondii harbors two phylogenetically distinct CDS enzymes

Our bioinformatic searches using *bona fide* CDS protein sequences from yeast and human identified one CDS gene in the *Toxoplasma* database (ToxoDB), termed as *Tg*CDS1 henceforth (ToxoDB, TGGT1_281980; GenBank™, KU199242). Similar database mining using the prokaryotic CDS sequences indicated the unexpected existence of a second CDS in the parasite, which was designated as *Tg*CDS2 (ToxoDB, TGGT1_263785; GenBank™ KU199243). Subsequently, we also found prokaryotic-type CDSs in selected protozoan parasites (*Eimeria falciformis*, *Trypanosoma cruzi*, and *Leishmania major*) albeit not in many others (*Plasmodium falciparum*, *Cryptosporidium parvum*, and *Trypanosoma brucei*). Phylogenetic clustering of CDS sequences revealed discrete eukaryotic and prokaryotic clades (Fig. 2*A*, supplemental Table S1). All eukaryotes possessed at least one CDS, which clustered with *Tg*CDS1. In contrast, *Tg*CDS2 segregated with prokaryotic-type CDS sequences from bacteria, plants, algae, and indicated parasites. Notably, *Tg*CDS2 grouped with CDSs from cyanobacteria (*Pm*CDS, *Ss*CDS, and *Te*CDS) and red alga (*Cc*CDS2 and *Gs*CDS2), both of which are considered as ancestors of the apicoplast in apicomplexan parasites (11, 14).

The ORFs of *Tg*CDS1 and *Tg*CDS2 encode for 1068 and 1044 amino acids with several transmembrane regions (Fig. 2*B*). Both proteins contain an archetypal cytidylyltransferase domain encompassing a CDS signature motif ($GX_4SX_2KRX_4KDX_5$ $PGHGGX_2DRXD$; Fig. 2, *B* and *C*). These features are shared by homologs from other organisms irrespective of the phylogenetic origins. Sequence comparisons also revealed many signature residues that were differentially conserved in the eukaryotic- and prokaryotic-type CDS motifs (see *red* and *blue-shaded* residues, Fig. 2*C*). In particular, the prokaryotic-type proteins harbor acidic and basic residues (aspartate-lysine) instead of small and aromatic pair of amino acids (glycine-phenylalanine) occurring in the eukaryotic-type orthologs. Likewise, eukaryotic CDSs show a strictly conserved nucleophile-amide motif (cysteine-glutamine) absent in prokaryotic counterparts. The cytidylyltransferase domain of *Tg*CDS1 exhibited a higher overall identity and similarity with the domains of other eukaryotic-type CDS sequences than with those of the prokaryotic types, whereas the reverse was true for *Tg*CDS2 (supplemental Table S1).

TgCDS1 is expressed in the ER, whereas TgCDS2 is expressed in the apicoplast

The parasite database indicated a constitutive expression of *Tg*CDS1 as well as *Tg*CDS2 transcripts during the lytic cycle (ToxoDB). To test whether *Tg*CDS1 and *Tg*CDS2 proteins are indeed expressed during the asexual development of tachyzoites, we tagged them with a HA epitope by 3′-insertional tagging of the endogenous loci (Fig. 2, *D* and *E*). The same approach also enabled us to determine subcellular distributions in intracellular parasites by immunofluorescence assays. Consistent with transcript abundance, endogenous expres-

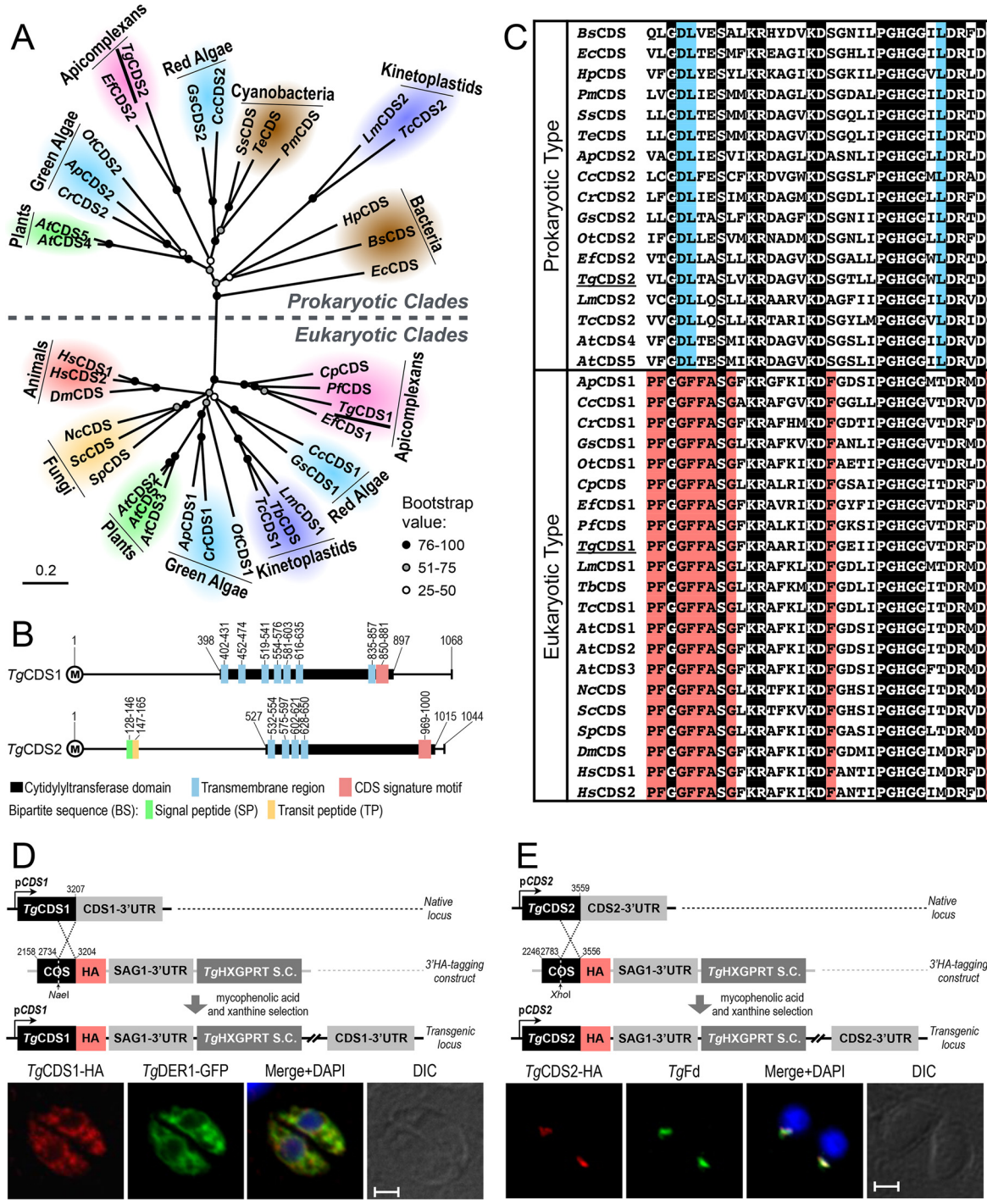

Figure 2. *T. gondii* expresses two distinct CDS enzymes located in the ER and apicoplast. *A*, phylogenetic analysis of *Tg*CDS1, *Tg*CDS2, and orthologs from various organisms representing major forms of life. Branch support was estimated by 100 bootstrap replicates. Other relevant information including the full names of organisms, accession numbers, identity, and similarity details for each CDS sequence are shown in supplemental Table S1. *B*, schematic drawing of the primary structures of *Tg*CDS1 and *Tg*CDS2. The *numbers* indicate positions of cytidylyltransferase domains, CDS signature motifs, and transmembrane regions as well as signal and transit peptides, as predicted by Simple Modular Architecture Research Tool (SMART), transmembrane hidden Markov model (TMHMM), SignalP 4.1, ChloroP 1.1, and PlasmoAP. *C*, multiple alignments of the signature motifs present in eukaryotic- and prokaryotic-type CDS sequences. The residues identical across all sequences are shaded in *black*, and amino acids that are conserved only in eukaryotes or prokaryotes are highlighted in *red* or *blue*, respectively. *D* and *E*, scheme for 3′-insertional tagging of *Tg*CDS1 and *Tg*CDS2 genes with a C-terminal HA tag. Plasmids harboring the COS of respective genes were linearized with the indicated enzymes and transfected into tachyzoites (RHΔ*ku80*-Δ*hxgprt*) followed by drug selection. Immunofluorescence of stable transgenic tachyzoites expressing *Tg*CDS1-HA (*D*) and *Tg*CDS2-HA (*E*) under the control of endogenous promoters and *Tg*SAG1–3′-UTR was performed using anti-HA and Alexa594 antibodies (24 h post-infection). *Tg*CDS1-HA and *Tg*CDS2-HA proteins were co-localized with *Tg*DER1-GFP signal and anti-*Tg*Fd/Alexa488 antibodies, respectively. *Scale bars*: 2 μm. *DIC*, differential interference contrast.

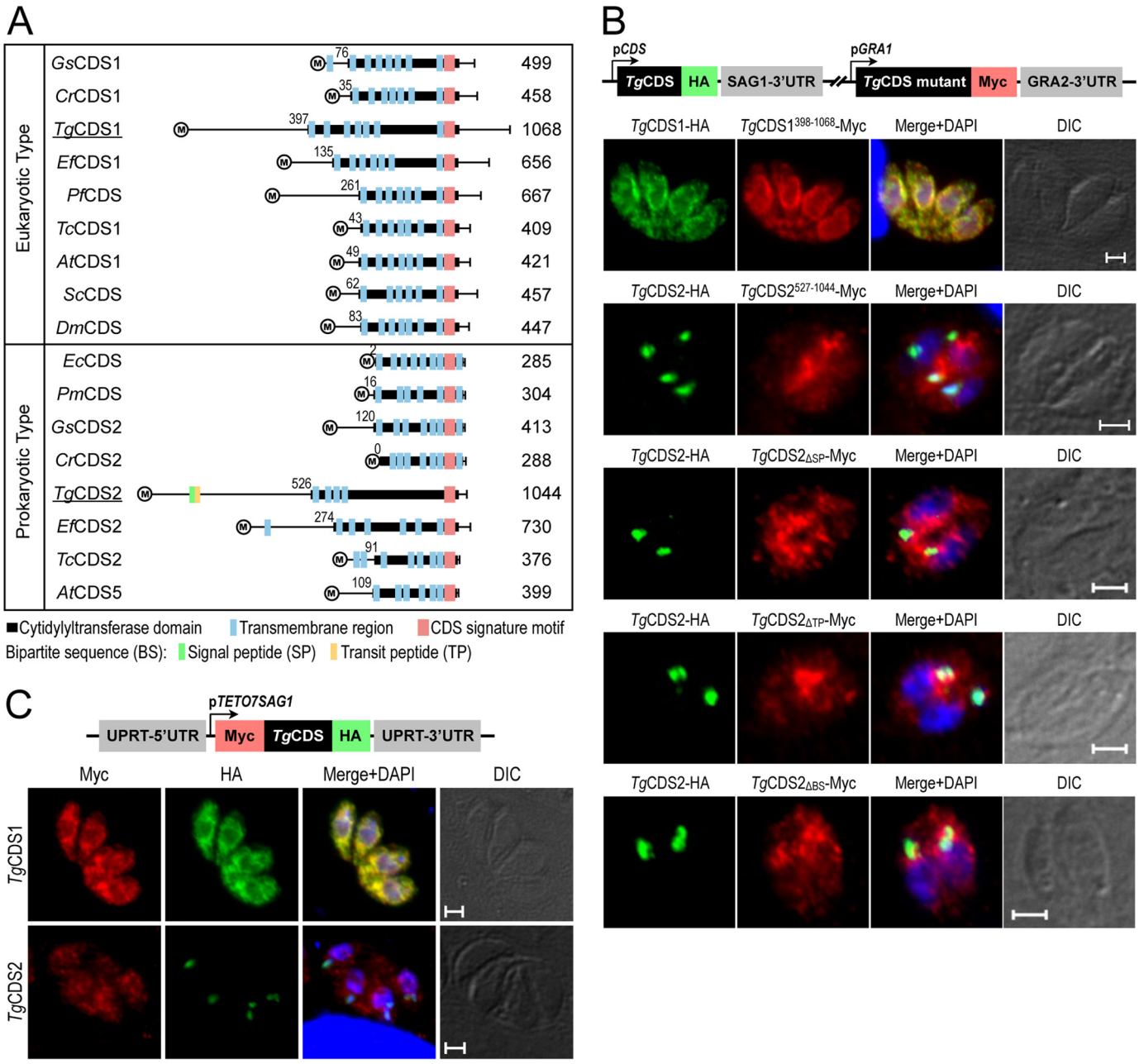

Figure 3. The N terminus of *Tg*CDS2, but not of *Tg*CDS1, is required for correct localization. *A*, comparison of the primary structures of CDS orthologs across different organisms. The *numbers* shown before cytidylyltransferase domains indicate the size of the N termini. The lengths of full-length proteins and the positions of the bipartite sequence in *Tg*CDS2 are also mentioned. *B*, immunofluorescence of tachyzoites co-expressing full-length CDS (*Tg*CDS1-HA or *Tg*CDS2-HA) along with corresponding truncated isoforms lacking the extended N-terminal region (*Tg*CDS1$^{398-1068}$-Myc or *Tg*CDS2$^{527-1044}$-Myc), signal peptide (*Tg*CDS2$_{\Delta SP}$-Myc), transit peptide (*Tg*CDS2$_{\Delta TP}$-Myc), or the entire bipartite sequence (*Tg*CDS2$_{\Delta BS}$-Myc). Transgenic parasites harboring epitope-tagged wild-type proteins (see Fig. 2, *D* and *E*, for details) were transfected with plasmids encoding the corresponding mutated isoforms (regulated by *Tg*GRA1 elements). *C*, immunofluorescence of intracellular parasites expressing dual-tagged CDS proteins (Myc-*Tg*CDS1-HA or Myc-*Tg*CDS2-HA) under the control of the p*TETO7SAG1* promoter. Immunostaining were performed 24 h post-infection using anti-HA/Alexa488 and anti-Myc/Alexa594 antibodies. *Scale bars*: 2 μm. *DIC*, differential interference contrast. *Gs*, *Galdieria sulphuraria*; *Cr*, *Chlamydomonas reinhardtii*; *Ef*, *Eimeria falciformis*; *Tc*, *Trypanosoma cruzi*; *At*, *Arabidopsis thaliana*; *Sc*, *Saccharomyces cerevisiae*; *Dm*, *Drosophila melanogaster*; *Ec*, *Escherichia coli*; *Pm*, *Prochlorococcus marinus*.

sion of *Tg*CDS1 and *Tg*CDS2 was readily detectable in stable transgenic strains. *Tg*CDS1-HA was expressed primarily in the parasite ER, as confirmed by its co-localization with a known organelle marker *Tg*DER1-GFP (15) (Fig. 2*D*). In contrast, *Tg*CDS2-HA co-localized with *Tg*Fd, a *bona fide* marker of the apicoplast (16) (Fig. 2*E*). Distinct subcellular locations of the two CDSs in *T. gondii* agree with their phylogenetic origins.

The alignment of primary structures revealed prolonged N-terminal extensions in *Tg*CDS1 and *Tg*CDS2 (Fig. 3*A*). Moreover, a putative bipartite sequence composed of a signal peptide and a transit peptide starting from the second methionine was identified in the N-terminal extension of *Tg*CDS2 (Fig. 3*A* and supplemental Fig. S1). To address the roles of extended N termini for subcellular targeting, the two mutant isoforms lacking the designated extensions and fused with a C-terminal

Myc tag (*Tg*CDS1$^{398-1068}$-Myc and *Tg*CDS2$^{527-1044}$-Myc) were ectopically expressed and co-localized with the corresponding full-length proteins. *Tg*CDS1$^{398-1068}$-Myc was still targeted to the ER, as discerned by co-staining with wild-type *Tg*CDS1 (Fig. 3*B*). In contrast, *Tg*CDS2$^{527-1044}$-Myc was not localized in the apicoplast anymore and appeared to be cytosolic instead (Fig. 3*B*), suggesting a crucial function of N-terminal peptide for correct location. We then generated additional mutants of *Tg*CDS2 protein containing internal deletions of either signal peptide (*Tg*CDS2$_{\Delta SP}$-Myc) or transit peptide (*Tg*CDS2$_{\Delta TP}$-Myc) or both (*Tg*CDS2$_{\Delta BS}$-Myc). Localization studies with these mutants revealed a clear role of bipartite sequence for targeting of *Tg*CDS2 to the apicoplast (Fig. 3*B*).

To examine whether the N termini were processed during maturation and targeting of the two proteins, we expressed dual-tagged isoforms containing a Myc tag at the N terminus and a HA epitope at the C terminus (Myc-*Tg*CDS1-HA or Myc-*Tg*CDS2-HA). In the case of *Tg*CDS1, both Myc and HA epitopes were distributed in the ER (Fig. 3*C*). However, the N-terminal region of *Tg*CDS2 (Myc-tagged) showed an evidently cytosolic signal, whereas the C-terminal peptide (HA-tagged) was still localized in the apicoplast (Fig. 3*C*), which suggested that the N terminus of the protein is cleaved off when the rest of the protein is imported and likely integrated into the organelle membrane.

CDS enzymes are indispensable for the lytic cycle of tachyzoites

To investigate the physiological importance of *Tg*CDS1 and *Tg*CDS2 in *T. gondii* tachyzoites, we first attempted to create mutants lacking either of the two genes. Our multiple endeavors to delete the *TgCDS1* and *TgCDS2* loci were futile, indicating essential nature of the two proteins in parasites. We, therefore, generated a conditional mutant of *Tg*CDS1 using the tetracycline repressor-based system as described elsewhere (17). To achieve the mutant, *Tg*CDS1-HA was first expressed under the control of a tetracycline-regulated promoter (p*TETO7SAG1*) targeted at the uracil phosphoribosyltransferase (*UPRT*) locus in the RHΔ*ku80*-TaTi strain (Fig. 4*A*, *Step 1*, making of a merodiploid strain). We then replaced the native *TgCDS1* locus by the dihydrofolate reductase-thymidylate synthase (DHFR-TS) selection cassette (S.C.) via double homologous recombination (Fig. 4*A*, *Step 2*, making of a Δ*tgcds1$_r$* mutant). Genetic deletion of the *Tg*CDS1 gene was confirmed by recombination-specific PCR screening, which showed the occurrence of 5′ and 3′ homologous recombination events in the mutant but not in the parental strain (Fig. 4*B*). RT-PCR validated a conditional repression of *Tg*CDS1 transcript by anhydrotetracycline (ATc) in the Δ*tgcds1$_r$* strain (Fig. 4*C*). *Tg*CDS1 mRNA was induced 2-fold under the control of p*TETO7SAG1* promoter, which could be down-regulated by ~14-fold in ATc-treated cultures. As shown by immunofluorescence and immunoblot analyses (Fig. 4, *D* and *E*), exposure to ATc also repressed the expression of *Tg*CDS1-HA protein, which was undetectable after 4 days of cultures with the drug.

Even though we were unsuccessful in generating a *Tg*CDS2 knock-out mutant using the parental strain, we were able to delete the *TgCDS2* locus in the Δ*tgcds1$_r$* mutant, which was probably due to overexpression of *Tg*CDS1 in the latter strain (Fig. 4*C*). To make a double mutant, a plasmid with the 5′ and 3′-UTRs of *Tg*CDS2 flanking the chloramphenicol acetyltransferase (CAT) S.C. was transfected in the Δ*tgcds1$_r$* strain (Fig. 4*A*, *Step 3*, making of a Δ*tgcds1$_r$*/Δ*tgcds2* mutant). The events of double homologous recombination and integration of the selection marker at the *TgCDS2* locus in the double mutant were verified by crossover-specific PCR (Fig. 4*B*). RT-PCR corroborated the absence of *Tg*CDS2 mRNA in the Δ*tgcds1$_r$*/Δ*tgcds2* strain (Fig. 4*C*). It was not feasible to test the protein level by immunofluorescence or immunoblot assays due to unavailability of antibody recognizing *Tg*CDS2. With respect to the transcriptional and translational regulation of *Tg*CDS1, the Δ*tgcds1$_r$*/Δ*tgcds2* mutant behaved similar to its parental Δ*tgcds1$_r$* strain (Fig. 4, *C–E*). For example, the Δ*tgcds1$_r$*/Δ*tgcds2* mutant also showed a 2-fold elevation of *Tg*CDS1 transcript in the *on state* (−ATc), which could be repressed by 14-fold in the *off state* (+ATc). Likewise, *Tg*CDS1 protein was expressed at comparable levels in both mutants (*on state*), and a chemical regulation was achievable within 96 h.

Conditional knockdown of TgCDS1 impairs biogenesis of PtdIns and PtdSer

To discern the functional importance of *Tg*CDS1 and *Tg*CDS2 for phospholipid synthesis, we performed lipidomic analysis. Lipids were isolated from tachyzoites of the parental, Δ*tgcds1$_r$* and Δ*tgcds1$_r$*/Δ*tgcds2* strains cultured in the absence or presence of ATc and subjected to high-performance liquid chromatography (HPLC) and mass spectrometry (MS). As anticipated, total phospholipids in the parental strain were not perturbed by treatment with ATc, whereas we found a modest increase in the Δ*tgcds1$_r$* mutant during *on state*, which was further increased in *off state* (Fig. 5*A*). In-depth analysis of individual lipids revealed a notable elevation of all major phospholipids, which were probably due to ectopic overexpression of *Tg*CDS1 (Figs. 5, *B–D*, and 6, *A* and *B*). More importantly, a knockdown of *Tg*CDS1 in the Δ*tgcds1$_r$* strain led to a significant and rather selective reduction in the amounts of PtdIns and PtdSer (Fig. 6, *A* and *B*), which was confirmed by thin-layer chromatography (not shown). Other phospholipids were either unaffected (PtdEtn, PtdThr, Fig. 5, *C* and *D*) or even elevated (PtdCho in Fig. 5*B*, PtdGro in Fig. 6*C*). Such a modest rise in PtdCho (accounting for >70% of total phospholipids; Refs. 2 and 3) was sufficient to induce the level of total lipids during *off state* despite a prominent decline in PtdIns and PtdSer (Fig. 5*A*), which together amounted to <10% of total phospholipids.

Next, we examined the major species of PtdIns and PtdSer (Fig. 6, *D* and *E*). PtdIns species were composed primarily of short to medium saturated and unsaturated fatty acids (30–36 carbons). In particular, the amount of the most plentiful species 34:1 and 34:2 in the Δ*tgcds1$_r$* mutant changed dramatically in an ATc-regulated manner when compared with the parental strain. Other key species of PtdIns that were declined upon repression of *Tg*CDS1 included 30:0, 32:1, and 36:2. One particular species 36:4 (C16:0/20:4) of PtdIns showed a surprisingly opposite trend in the mutant. Interestingly, the most abundant PtdIns species in human foreskin fibroblasts (HFFs) is PtdIns 38:4 (C18:0/20:4), which is negligible in the parasite extract (<3% of total PtdIns) leading to a suspicion that

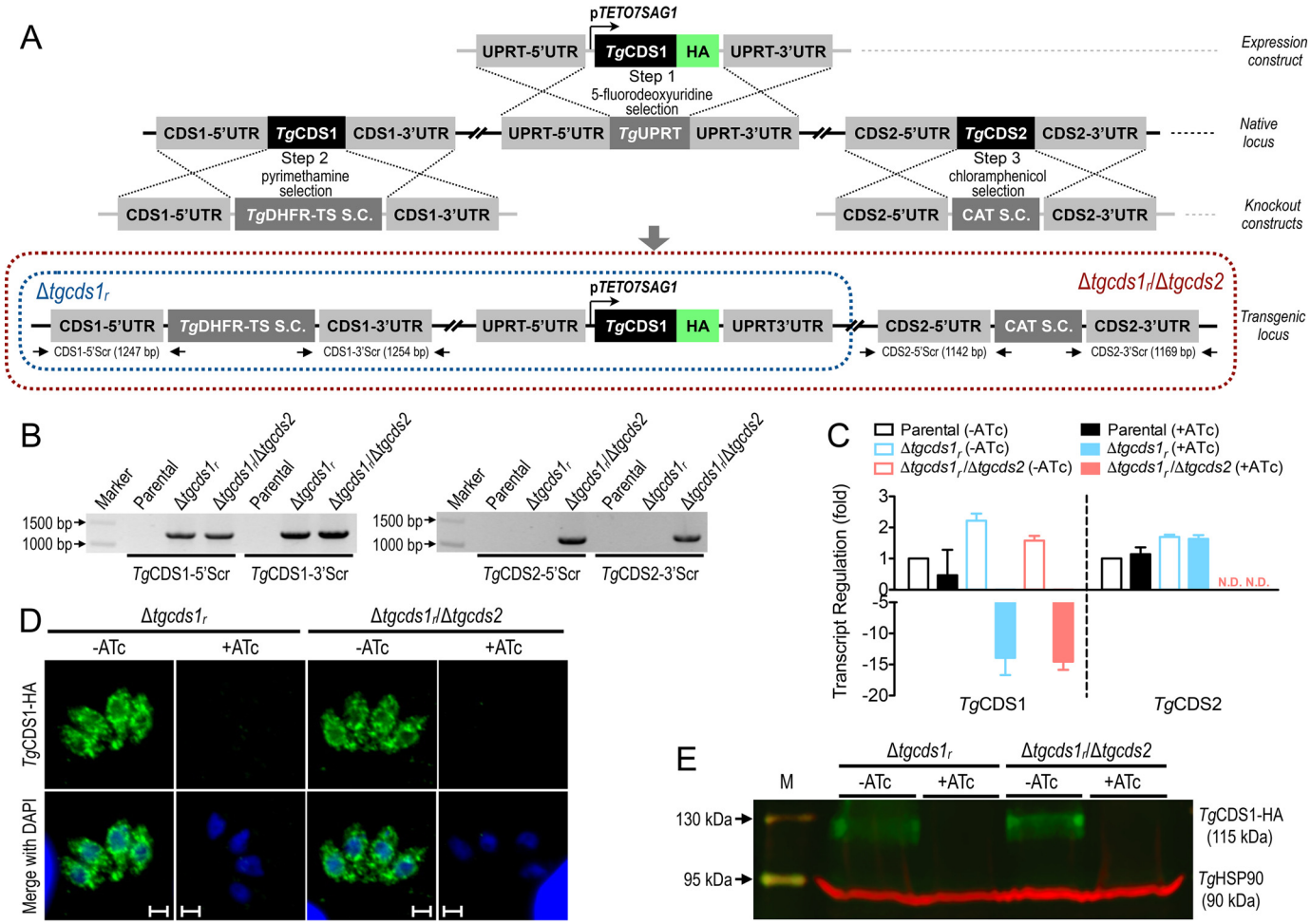

Figure 4. Conditional mutagenesis of *Tg*CDS1 and deletion of *Tg*CDS2 in *T. gondii*. *A*, scheme for creating the Δ*tgcds1*$_r$ and Δ*tgcds1*$_r$/Δ*tgcds2* mutants. *Steps 1* and *2* depict the making of the Δ*tgcds1*$_r$ mutant, which involved integrating a tetracycline-regulatable copy of *Tg*CDS1 (*Tg*CDS1-HA) at the *TgUPRT* locus in the RHΔ*ku80*-TaTi strain (*Step 1*) followed by deletion of the *TgCDS1* gene by the *Tg*DHFR-TS S.C. via double homologous recombination (*Step 2*). Subsequently, to generate the Δ*tgcds1*$_r$/Δ*tgcds2* strain (*Step 3*), the *TgCDS2* gene was deleted in the Δ*tgcds1*$_r$ mutant by the CAT selection marker. Primers used to screen for 5′ and 3′ recombination at the *TgCDS1* and *TgCDS2* loci are marked as *arrows*. *B*, genomic PCR of the Δ*tgcds1*$_r$ and Δ*tgcds1*$_r$/Δ*tgcds2* strains confirming the events of 5′ and 3′ crossovers. Genomic DNA of the parental strain was included alongside (negative control). *C*, quantitative PCR of *Tg*CDS1 and *Tg*CDS2 transcripts in the Δ*tgcds1*$_r$ and Δ*tgcds1*$_r$/Δ*tgcds2* mutants. The *Tg*CDS1 transcript was repressed 14-fold in the *off state* (+ATc). *Tg*CDS2 transcript was not detectable (*N.D.*) in the Δ*tgcds1*$_r$/Δ*tgcds2* strain. The average values with S.E. from three independent assays are shown. *D* and *E*, immunofluorescence and immunoblot analyses of the two mutants showing a conditional regulation of *Tg*CDS1-HA by ATc. Staining was performed using anti-HA and anti-*Tg*HSP90 antibodies (loading control). *Scale bars*: 2 μm.

tachyzoites might salvage this species containing the C20:4 acyl chain from host cells and then remodel it to its own benefit. The most abundant PtdSer species contained mono- and polyunsaturated acyl chains with 34, 36, and 42 carbon atoms. All of them were induced noticeably during *on state* of the Δ*tgcds1*$_r$ strain and reduced after a down-regulation of *Tg*CDS1 (*off state*). These data together suggest a requirement of *Tg*CDS1 to produce PtdIns and PtdSer via CDP-DAG-dependent enzymes.

Loss of TgCDS2 results in a selective impairment of PtdGro synthesis

Having evaluated the impact of *Tg*CDS1 knockdown in the single mutant, we examined a role of *Tg*CDS2 for phospholipid biogenesis and functional interrelationship of both enzymes using the Δ*tgcds1*$_r$/Δ*tgcds2* strain. In essence, biochemical phenotypes of the double mutant were similar to the parental and Δ*tgcds1*$_r$ strains with few noteworthy exceptions. One of the most evident effects was >80% reduction in PtdGro biogenesis upon ablation of *Tg*CDS2 (Fig. 6*C*). All species of PtdGro were significantly decreased irrespective of ATc treatment, which confirmed a need of *Tg*CDS2 (but not *Tg*CDS1) for PtdGro biogenesis (Fig. 6*F*). Consistently, the most common PtdGro species with short saturated fatty acids (30:0) was increased when *Tg*CDS1 was repressed in the Δ*tgcds1*$_r$ strain (Fig. 6*F*), suggesting utilization of subsequently surplus PtdOH species into PtdGro via *Tg*CDS2. Cardiolipin was detectable only in the minor amounts even in the parental strain; we were, therefore, unable to reproducibly quantify and compare its levels across the parasite strains. The deletion of *Tg*CDS2 in the Δ*tgcds1*$_r$ strain also resulted in an apparent diminution of certain PtdIns (34:2, 30:0) and PtdSer (34:2) species in the Δ*tgcds1*$_r$/Δ*tgcds2* mutant during *on state*, which were further reduced by deficiency of *Tg*CDS1 in *off state* (Fig. 6, *D* and *E*). Other major lipids were largely unaffected by loss of *Tg*CDS2 when compared with the parental strain (Fig. 5).

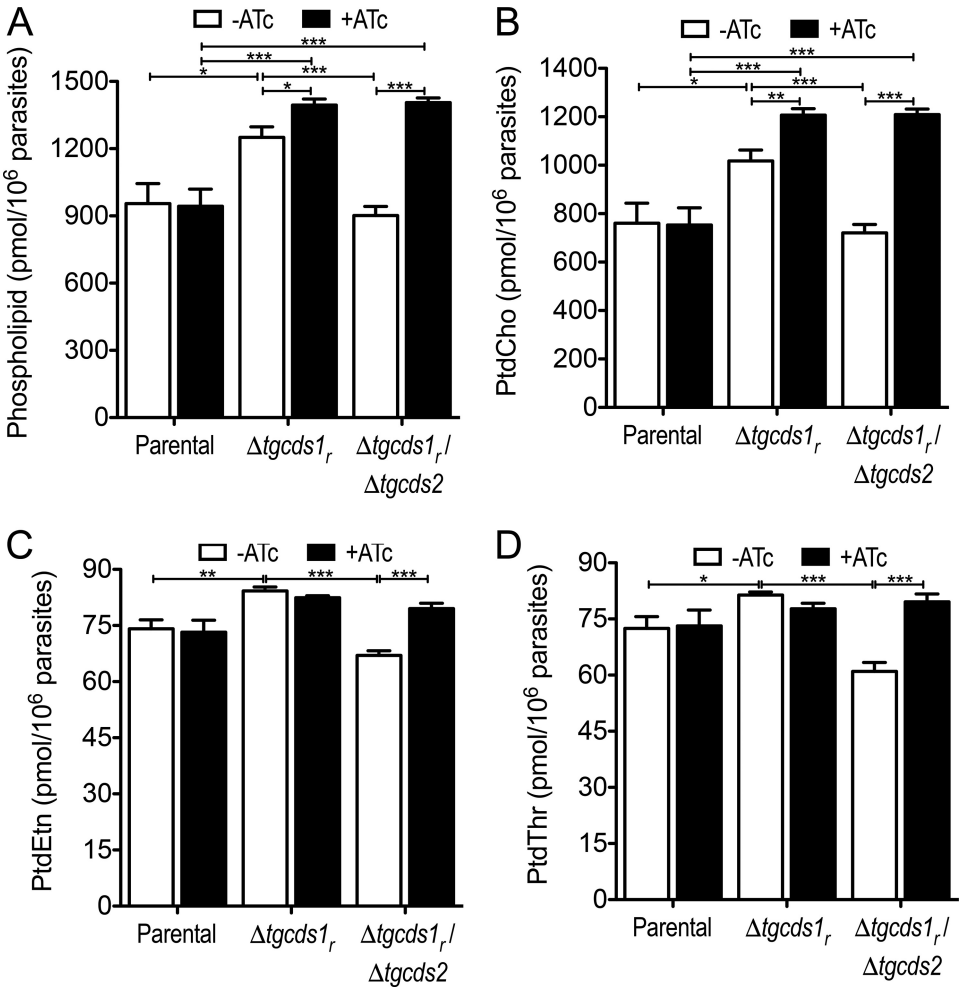

Figure 5. Phospholipid profiles of the Δ*tgcds1*$_r$ and Δ*tgcds1*$_r$/Δ*tgcds2* strains. Lipids isolated from tachyzoites were analyzed by HPLC/MS. Major phospholipids identified were PtdCho, PtdEtn, PtdThr, PtdIns, PtdSer, and PtdGro. *A* shows the cumulative sum of all lipids in the indicated strains cultured with or without ATc. Other panels illustrate PtdCho (*B*), PtdEtn (*C*), and PtdThr (*D*). PtdIns, PtdSer, and PtdGro are depicted in Fig. 6. Values are the means with S.E. from six independent assays (*, $p < 0.05$; **, $p < 0.01$; ***, $p < 0.001$).

The CDS mutants show a defective growth due to impaired replication

We next determined the phenotypic effects of *Tg*CDS1 knockdown and *Tg*CDS2 knock-out on the lytic cycle of tachyzoites in HFF cells. To measure the growth fitness, we first performed plaque assays, which recapitulate the consecutive lytic cycles of tachyzoites (Fig. 7*A*). The two mutants along with the parental strain were cultured in the absence or presence of ATc. The Δ*tgcds1*$_r$ strain demonstrated normal growth during *on state*, whereas plaque size was reduced down to 25% in *off state* when compared with the parental strain (Fig. 7*B*). Plaque formation by the Δ*tgcds1*$_r$/Δ*tgcds2* strain declined by a modest 12% during the *on state* with respect to the parental strain and was severely reduced by ~90% when the expression of *Tg*CDS1 was turned off (Fig. 7*B*). Plaque numbers of both mutants were the same as the parental strain in *on state*, as expected, whereas they dropped down to ~60 and 40% during *off state*, respectively (Fig. 7*C*). The addition of exogenous CDP-DAG, PtdIns, PtdGro, and cardiolipin to the plaque cultures did not restore the growth of either of the mutants (not shown), indicating that tachyzoites are unable to scavenge these lipids from the surrounding milieu.

A similar phenotype of the mutants was observed in yield assays when parasites were syringe-released and counted 40 h post-infection (Fig. 7*D*). The parasite yield dropped by 75%, 23%, and 96% after the loss of *Tg*CDS1 (*off-state* Δ*tgcds1*$_r$), *Tg*CDS2 (*on-state* Δ*tgcds1*$_r$/Δ*tgcds2*) alone, or both (*off-state* Δ*tgcds1*$_r$/Δ*tgcds2*), respectively. Based on the parasite yields, we also calculated the replication rate of all strains. The doubling time of the parental strain was ~9.4 h, which was prolonged to 16.2 h when *Tg*CDS1 expression was knocked down in the Δ*tgcds1*$_r$ mutant. Knock-out of *Tg*CDS2 alone caused only a modest delay in cell division (10.2 h). However, a loss of both enzymes severely attenuated the parasite proliferation (doubling time, 56.5 h). We also assessed the replication by numerating parasites in the parasitophorous vacuoles (Fig. 7*E*). We found an evident downshift in the vacuole sizes of both strains after treatment with ATc. In other words, mutants in *off state* contained a higher proportion of smaller vacuole, whereas the converse was true for *on state*.

A deficiency of CDP-DAG synthesis attenuates the parasite virulence

We then investigated the physiological relevance of CDP-DAG synthesis within the parasite for virulence in a mouse

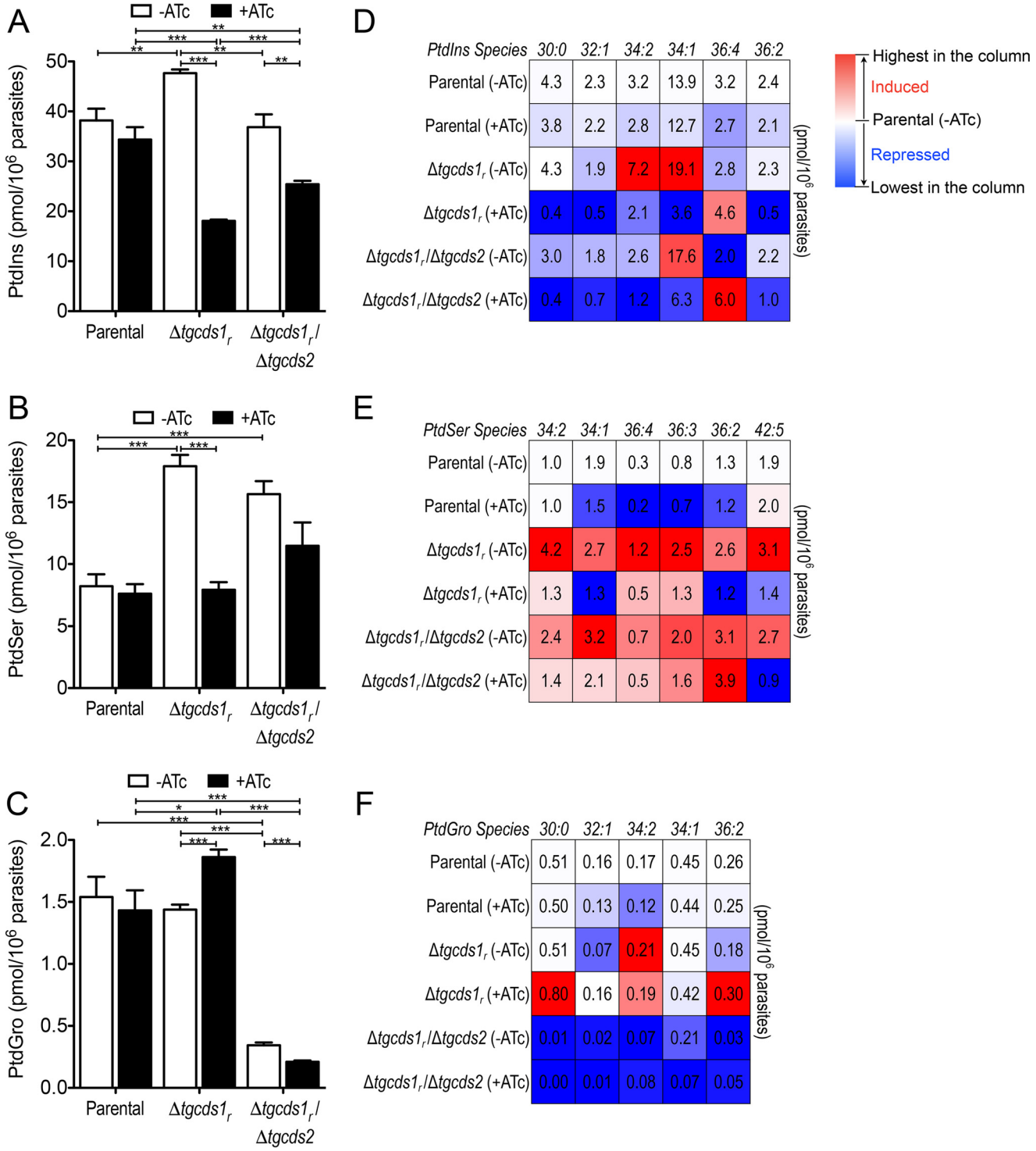

Figure 6. Conditional knockdown of *Tg*CDS1 results in a reduction of PtdIns and PtdSer, whereas deletion of *Tg*CDS2 impairs PtdGro biogenesis. Total lipids were extracted from tachyzoites of the indicated strains and subjected to HPLC and MS analysis. Amounts of PtdIns (*A*), PtdSer (*B*), PtdGro (*C*), and the corresponding major lipid species (*D*, *E*, and *F*) in the presence or absence of ATc are depicted in heat-maps. The color-coded gradient in each column is meant to compare the relative abundance of the given lipid species in the mutants with respect to the *on-state* parental strain. Actual amounts of lipid species (pmol/10^6 parasites) are also mentioned for comparing columns. The sums of individual lipid species in *D–F* are less than the total lipid amount in *A–C* because only major species are shown. Note that the reduction of PtdSer species in the *off-state* parental strain (+ATc) is relatively negligible even though they appear somewhat blue. All values show the mean values with S.E. from six independent assays (*, $p < 0.05$; **, $p < 0.01$; ***, $p < 0.001$).

model (Fig. 7*F*). In this regard we employed the Δ*tgcds1*$_r$ mutant along with the parental strain. Our rationale for using only the single mutant was based on a robust phenotypic impairment observed *in vitro* (*off state*, Fig. 7, *A–E*), which should ideally translate into a strong weakening of virulence *in vivo*. Hence, a double mutant (Δ*tgcds1*$_r$/Δ*tgcds2*) with even more inhibited *in vitro* growth would be more attenuated *in vivo*. Indeed, most animals infected with the Δ*tgcds1*$_r$ strain that

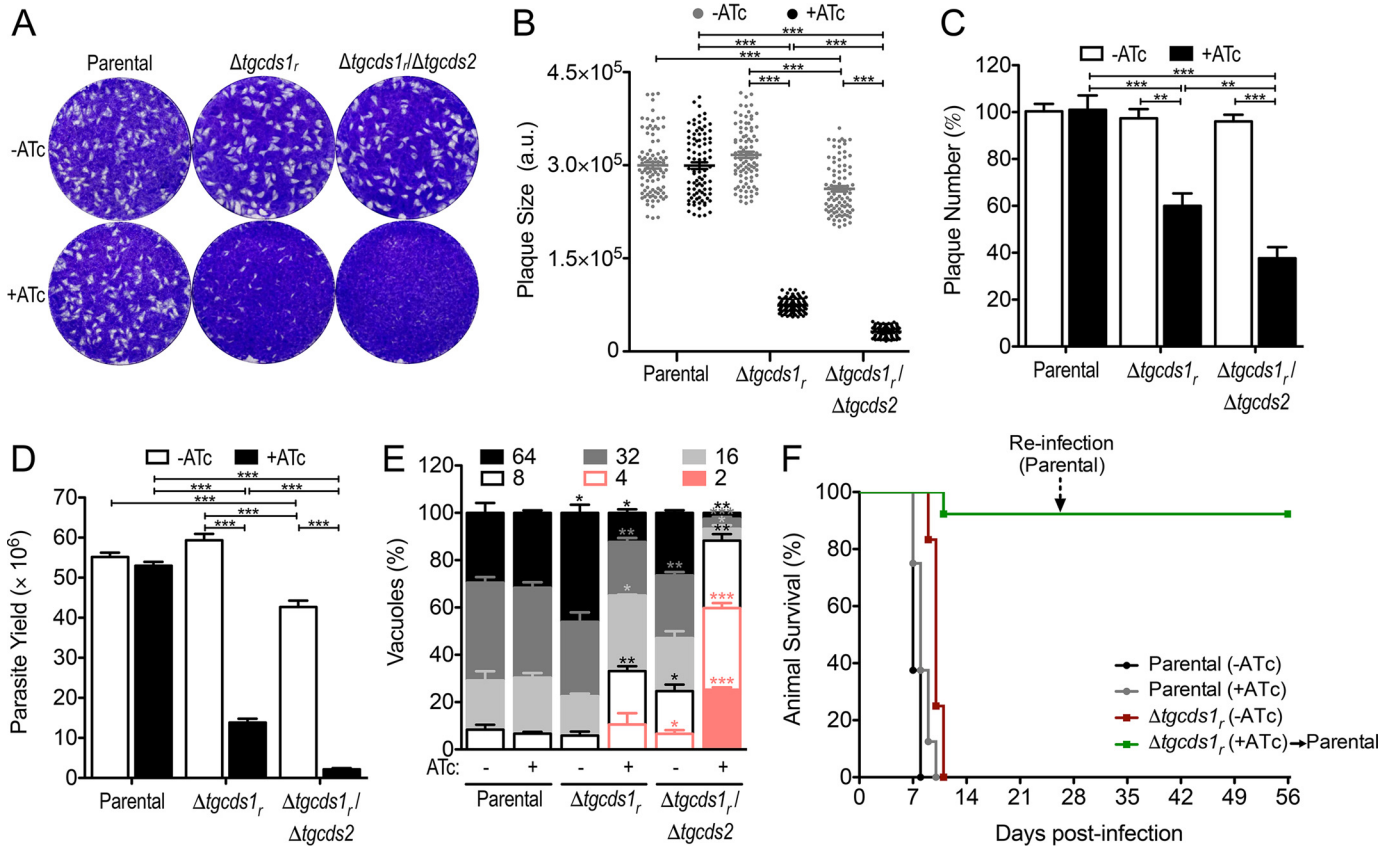

Figure 7. The Δ*tgcds1*$_r$ and Δ*tgcds1*$_r$/Δ*tgcds2* mutants show an attenuated growth. *A*, plaque assays using the indicated parasite strains cultured in the presence or absence of ATc. HFF monolayers were infected with 250 tachyzoites (pre-cultured with or without ATc for 4 days) and incubated for 1 week without any perturbation to allow plaque formation. *B*, plaque sizes of the parasite strains from *A*. 90 plaques of each strain were measured for area using the ImageJ software. *a.u.*, arbitrary units. *C*, plaque numbers of individual strains from *A*. *D*, yield assays in the presence or absence of ATc. Host cells were infected with 3 million tachyzoites pretreated with ATc for 4 days before the assay (m.o.i. 3). Parasites were syringe-released 40 h post-infection for counting. *E*, replication assays in HFFs (m.o.i. 1). Cells were fixed 40 h post-infection and stained with anti-*Tg*GAP45 antibody to visualize intracellular tachyzoites. A total of 100–150 vacuoles were analyzed for each strain. The percentages of vacuoles containing different numbers of parasites are shown. Values are the means with S.E. for three (*B*, *C*, and *E*) or six (*D*) independent experiments (*, $p < 0.05$; **, $p < 0.01$; ***, $p < 0.001$). *F*, virulence assay in a mouse model. Animals (C57BL/6J) were infected intraperitoneally with tachyzoites (10^3) of the parental or Δ*tgcds1*$_r$ strains (pre-cultured with or without ATc for 6 days). Drug treatment during infection (2 weeks) was performed via the drinking water. Infected mice were monitored for 28 days (2 assays, each with 4 mice for the parental strain and 6 mice for the Δ*tgcds1*$_r$ strain). Animals surviving infection with the mutant strain (+ATc) were challenged with the parental strain (10^3, *dotted arrow*) and examined for additional 28 days.

were treated with ATc in drinking water survived, as opposed to the control parental strain, which was categorically lethal irrespective of ATc treatment. The mutant in its *on state* exhibited a lethal phenotype similar to the parental strain. Collectively, these results indicated an essential role of CDS for the lytic cycle and virulence in mice. The data also suggested that tachyzoites are unable to salvage sufficient amounts of CDP-DAG from the host to bypass an ablation of autonomous synthesis. We also explored the vaccination potential of the Δ*tgcds1*$_r$ strain. Notably, all animals surviving the primary infection with the mutant developed sufficient immunity to resist the subsequent lethal challenge by a hypervirulent strain, which proves the prophylactic utility of a metabolically attenuated mutant to prevent acute toxoplasmosis.

PtdGro phosphate and PtdIns are made in the mitochondrion and Golgi bodies, respectively

The CDS-dependent synthesis of PtdIns and PtdGro resonates with the occurrence of a PtdIns synthase (PIS) and a PtdGro phosphate (PtdGro-P) synthase (PGPS) in tachyzoites. The second enzyme of PtdGro synthesis (PtdGro-P phosphatase) could not be identified in the parasite genome. We examined subcellular distribution of *Tg*PGPS (ToxoDB, TGGT1_246530; GenBank™, KX017550) by 3′-HA tagging of the endogenous locus in *T. gondii*. *Tg*PGPS-HA was expressed in the parasite mitochondrion, as shown by its co-staining with a *bona fide* organelle marker *Tg*F1B (7) (Fig. 8*A*). We also immuno-localized *Tg*PIS-HA (ToxoDB, TGGT1_207710; GenBank™, KX017549). It co-localized with a known marker of the Golgi body *Tg*ERD2 (Fig. 8*B*). Taken together, these results indicated synthesis of PtdGro and PtdIns in the mitochondrion and Golgi, respectively, requiring a transfer of CDP-DAG from the apicoplast and ER to the sites of phospholipid biogenesis.

Discussion

This study identified two phylogenetically distinct enzymes involved in the synthesis of one of the central lipid precursors CDP-DAG in *T. gondii*. *Tg*CDS1 belongs to the eukaryotic-type CDSs that are conserved across the eukaryotic organisms. It is compartmentalized in the ER of tachyzoites, similar to what has been described for corresponding CDS proteins in yeast (18), plants (19), and mammals (20, 21). In protozoan parasites *P. falciparum* and *T. brucei*, only one eukaryotic-type CDS has

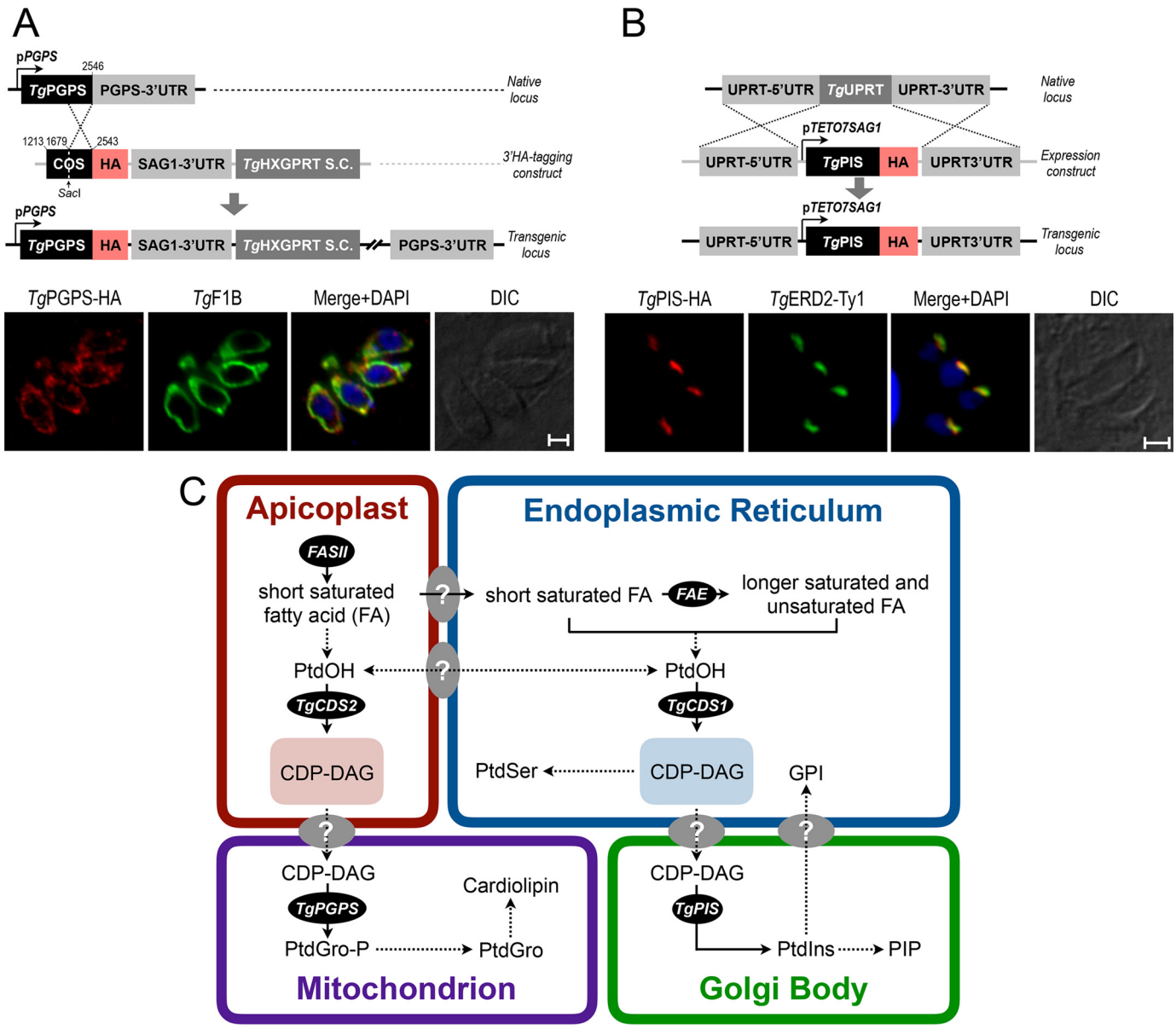

Figure 8. CDP-DAG-dependent biogenesis of PtdIns, PtdSer and PtdGro in the tachyzoite stage of *T. gondii*. *A* and *B*, immunofluorescent images of intracellular tachyzoites expressing either *Tg*PGPS-HA or *Tg*PIS-HA regulated by endogenous and p*TETO7SAG1* elements, respectively. The indicated proteins were localized 24 h post-infection using anti-HA antibody and corresponding co-localization markers (*Tg*F1B, *Tg*ERD2-Ty1). 3′-Insertional tagging was performed as described in Fig. 2, *D* and *E*. *Scale bars*: 2 μm. *DIC*, differential interference contrast. *C*, a model of lipid biogenesis embodying division of labor among the specified organelles in tachyzoites. The illustration depicts abridged interorganelle trafficking of selected lipids, especially those relevant to the context. Two distinct CDP-DAG sources are utilized to produce PtdIns, PtdSer, and PtdGro. The CDP-DAG pool in the ER is generated by *Tg*CDS1 and used for biogenesis of PtdIns in the Golgi bodies. PtdIns should enable the synthesis of phosphatidylinositol phosphates (*PIP*) and glycosylphosphatidylinositol (*GPI*). *Tg*CDS2 generates a second pool of CDP-DAG in the apicoplast that contributes to the making of PtdGro and cardiolipin in the mitochondrion. The confirmed pathways are marked with *solid arrows*, whereas those hypothesized are shown with *dotted arrows*. *FASII*, fatty acid synthase type II; *FAE*, fatty acid elongase.

been identified, which is required for the biosynthesis of PtdIns and its descendant lipid glycosylphosphatidylinositol (22–24). In mammals and plants there are two or more eukaryotic-type CDS enzymes with different expression patterns, all of which influence PtdIns and PtdOH levels (19, 25). Interestingly, a mitochondrial maintenance protein lacking the typical cytidyltransferase domain and CDS signature motif (Tam41) was found to catalyze the formation of CDP-DAG from PtdOH in the yeast mitochondria (26); however, similar proteins have not been identified in any protozoan parasites. Instead, we discovered a prokaryotic-type *Tg*CDS2 in the apicoplast of *T. gondii* and its orthologs in selected protozoan parasites, *e.g. E. falciformis*, *T. cruzi*, and *L. major*. No homologs were found in *P. falciparum*, *C. parvum*, and *T. brucei*, suggesting a loss of the prokaryotic-type CDS during the evolution of these parasites.

Apicoplast has evolved by two successive endosymbiotic events, first involving cyanobacteria and then red alga (11, 14, 27–29). Both events were ensued by horizontal gene transfer from the cyanobacterial genome to the algal genome and subsequently to the genome of the parasites. As a result, most of the apicoplast proteins, including *Tg*CDS2, have prokaryotic or algal origins but are encoded by the parasite nucleus (14, 30, 31). Endosymbiotic gene transfer from the apicoplast to the nucleus enables parasites to control the foreign organelle; however, it

requires post-translational targeting of proteins back to the apicoplast. In many apicoplast-resident proteins, this process is guided by an N-terminal bipartite sequence comprising a signal peptide and a transit peptide (32). These proteins are first imported into the ER and then transferred directly from the ER to the apicoplast either through the general secretory pathway or via vesicular trafficking (33–35). Recent studies also reveal involvement of the Golgi as a sorting point for soluble proteins destined to the apicoplast (36, 37). Both putative signal and transit peptides could be identified in the N terminus of the *Tg*CDS2 sequence; however, they begin from the second methionine instead of the start codon. Consistently, our mutagenesis studies confirm the need of prolonged N-terminal extension and bipartite sequence for localization in the apicoplast. The data indicate that the targeting of *Tg*CDS2 to the apicoplast is mediated by the bipartite signal mechanism.

*Tg*CDS1 and *Tg*CDS2 mutants showed severely reduced growth and attenuated virulence, which is associated with the loss of PtdIns and PtdGro in parasites. PtdIns serves not only as a structural component of membranes but also as a precursor for the biogenesis of central signaling molecules. Earlier studies on the PtdIns phosphates have revealed that PtdIns 3-monophosphate and PtdIns 3,5-bisphosphate are required for the apicoplast biogenesis in tachyzoites (38, 39). Another downstream product of PtdIns, glycosylphosphatidylinositol, has been implicated in host-cell attachment and modulation of immune response and is reported to be essential for the parasite survival (40, 41). By contrast, literally nothing is known about the structural and functional relevance of PtdGro in *T. gondii*. PtdGro typically serves as an intermediate for the synthesis of cardiolipin, which is indispensable for the mitochondrial homeostasis and viability of kinetoplastid parasites (42, 43). It is expected that changes in PtdIns, PtdGro, and cardiolipin would result in organelle dysfunction and eventual demise of *T. gondii* unless parasites could salvage CDP-DAG or its descendent lipids from the host cell to bypass the ablation of CDS enzymes, which seems not to be the case. Detailed biochemical and morphological analyses shall reveal the underlying basis of the growth impairment in the CDS mutants.

*Tg*CDS1 and *Tg*CDS2 mutants did not show a perturbation of other dominant phospholipids except for PtdCho, which can be explained by the endogenous pathways expressed in tachyzoites. We have previously reported the functional existence of PtdCho and PtdEtn syntheses in the ER through CDP-choline and CDP-ethanolamine pathways, respectively, both of which utilize DAG as the lipid backbone (2, 6, 7). Because synthesis of PtdCho occurs exclusively through the CDP-choline route, a significant increase in the lipid content during the *off state* of the two mutants is expected due to potential rerouting of PtdOH to DAG. On the other hand, PtdEtn can also be produced by decarboxylation of PtdSer in the parasite mitochondrion and parasitophorous vacuole (5, 7), which may have balanced its content in the single and double mutants. PtdSer and PtdThr are generated from PtdEtn and/or PtdCho in a base-exchange manner by two distinct routes located in the parasite ER (4). No change of PtdThr was observed in both mutants. Given its unique fatty acid chain composition (mostly 20:1, 20:4), it seems that a different source of glycerol backbone or lipid remodeling is required to make PtdThr. In the case of PtdSer, a sizeable increase during *on state* and a decline in *off state* of both mutants was surprising and suggests the presence of yet another PtdSer synthase (CDP-DAG-dependent) for making PtdSer (Fig. 8*C*). A perturbation in the amounts of PtdCho and PtdSer may also account for the phenotype observed in individual mutants. Although the detection of CDP-DAG and DAG in tachyzoite has been quite challenging, future studies using isotope labeling with lipid precursors (polar head groups, glycerol) should validate aforesaid postulations.

*Tg*CDS1 and *Tg*CDS2 are utilized for biogenesis of PtdIns, PtdSer, and PtdGro in a rather selective manner. Our data suggest a model in which ER-derived CDP-DAG fuels the synthesis of PtdIns in the Golgi bodies, whereas CDP-DAG originating in the apicoplast is utilized for making PtdGro in the mitochondrion (Fig. 8*C*). These data are consistent with the presence of two isoforms of each enzyme synthesizing lysophosphatidic acid and phosphatidic acid (ToxoDB). One such enzyme, glycerol-3-phosphate acyltransferase, has recently been reported to localize in the apicoplast (44), whereas others remain to be characterized. Such a spatial distribution of lipid syntheses necessitates a coordinated lipid transport among organelles in *T. gondii*. It will be interesting to examine the topological orientations of these enzymes in different organelles, which is imperative for a concerted lipid synthesis. Several lipid trafficking mechanisms have been reported, especially in yeast and mammalian cells, which involve lateral and transbilayer movements within the same organelle as well as membrane contact sites, vesicular trafficking, and protein-mediated transport between different organelles (45–47). In apicomplexan parasites, analogous membrane contact sites have been observed between the ER, Golgi body, apicoplast, and mitochondrion (48, 49); however, whether they serve as the privileged zones of inter-organelle exchange merits further investigation, in particular a "retrograde" transfer of PtdIns from Golgi to ER and of CDP-DAG from ER/apicoplast to Golgi/mitochondrion. Our prototype model of lipid synthesis and trafficking provides a framework for studying the paradigm in a well established model eukaryotic pathogen.

Experimental procedures

Biological reagents and resources

The RHΔ*ku80*-TaTi (30) and RHΔ*ku80*-Δ*hxgprt* (50) strains of *T. gondii* were kindly provided by Boris Striepen (University of Georgia) and Vern Carruthers (University of Michigan). The *pG152, pTKO-HXGPRT*, and *pTUB8-TgDER1-GFP* plasmids were donated by Markus Meissner (University of Glasgow), John Boothroyd (Stanford University School of Medicine), and Boris Striepen (University of Georgia), respectively. The *pTKO-CAT* and *pTKO-DHFR-TS* plasmids were generated by modifying the *pTKO-HXGPRT* plasmid. Primary antibodies against *Tg*Fd, *Tg*HSP90, *Tg*GAP45, *Tg*SAG1, and *Tg*F1B proteins were provided from Frank Seeber (Robert-Koch Institute, Berlin), Sergio Angel (IIB-INTECH, Chascomús, Argentina), Dominique Soldati-Favre (University of Geneva), Jean-Francois Dubremetz (University of Montpellier), and Peter Bradley (University of California, Los Angeles, CA), respectively. Other

primary antibodies (anti-HA, Myc or Ty1) were purchased from Sigma. Secondary antibodies (Alexa488 or Alexa594) as well as oligonucleotides were supplied from Life Technologies.

Parasite and host cell cultures

HFFs (Cell Lines Service, Eppelheim, Germany) were cultured in DMEM supplemented with 10% fetal bovine serum (PAN Biotech, Aidenbach, Germany), 2 mM glutamine, 1 mM sodium pyruvate, minimum Eagle's non-essential amino acids, 100 units/ml penicillin, and 100 μg/ml streptomycin in a humidified incubator (37 °C, 5% CO_2). HFFs were harvested by trypsinization and grown to confluence in flasks, dishes, or plates as required. Tachyzoites were propagated by serial passage in HFF monolayers at a m.o.i. of 3. For all assays including lipidomics, parasites were mechanically released from late-stage cultures and used immediately. Briefly, parasitized cells (40–42 h infection) were scraped in fresh culture medium and squirted through 23- and 27-gauge syringes (2× each) to obtain extracellular tachyzoites for the experiments described herein.

Molecular cloning and real-time PCR

RNA was isolated from freshly syringe-released tachyzoites using TRIzol-based extraction method and subsequently reverse-transcribed into first-strand cDNA (Life Technologies). The gDNA was isolated using the genomic DNA preparation kit (Jena Bioscience, Jena, Germany). All amplicons were amplified by Pfu Ultra II Fusion polymerase (Agilent Technologies, Santa Clara, CA) and cloned into the corresponding vectors either by ligation-independent or by restriction enzyme-mediated cloning as indicated. Primers used for PCRs are listed in supplemental Table S2. Plasmids were transformed into *Escherichia coli* XL-1b strain for cloning and vector amplification. To perform the real-time PCR, total RNA was first reverse-transcribed using the oligo-dT primer and analyzed by SYBR Green-based assays (Mastercycler Pro Gradient S System, Eppendorf, Hamburg, Germany). The relative expression of transcripts (-fold induction) was calculated with respect to the parental strain using the ΔΔCT method. Transcripts of elongation factor A, tubulin A, and glucose transporter 1 were used as housekeeping genes to examine the normalized expression of *Tg*CDS1 and *Tg*CDS2 across samples.

Generation of transgenic parasites

For generating the transgenic strains, the respective plasmid constructs were transfected into fresh tachyzoites of specified strains suspended in filter-sterile Cytomix (120 mM KCl, 0.15 mM $CaCl_2$, 10 mM K_2HPO_4/KH_2PO_4, 25 mM HEPES, 2 mM EGTA, 5 mM $MgCl_2$, 5 mM glutathione, 5 mM ATP, pH 7.6) using a BTX electroporation instrument (50 μg of plasmid DNA, ~10^7 parasites, 2 kV, 50 ohms, 25 microfarads, 250 μs). Transformed tachyzoites were selected for resistance to a drug corresponding to the selection marker encoded by transfected plasmid. The drug-resistant transgenic parasites were cloned by limiting dilution, and individual clones were screened by PCR and/or immunofluorescence assays.

For tagging of the *Tg*CDS1, *Tg*CDS2, and *Tg*PGPS genes with a C-terminal HA tag, 1.0–1.3 kb of the 3′-end of these genes excluding stop codon (crossover sequence (COS)) were amplified using tachyzoite gDNA and gene-specific primers (supplemental Table S2). Amplicons were inserted into the *pG152* vector by ligation-independent cloning. Constructs were linearized using an appropriate enzyme (NaeI, XhoI, or SacI as specified in figures) present in the COS and transfected into the RHΔ*ku80*-Δ*hxgprt* strain. Parasites were selected for hypoxanthine-xanthine-guanine phosphoribosyltransferase (HXGPRT) expression using mycophenolic acid (25 μg/ml) and xanthine (50 μg/ml) (51). The resulting transgenic strains expressed *Tg*CDS1-HA, *Tg*CDS2-HA, or *Tg*PGPS-HA under the control of conforming endogenous promoters and 3′-UTR of *Tg*SAG1. Parasites expressing *Tg*CDS1-HA were subsequently transfected with the construct encoding for *Tg*DER1-GFP (regulated by p*TUB8* promoter) for co-localization studies.

For ectopic expression of $TgCDS1^{398-1068}$-Myc (lacking N-terminal extension and tagged with a C-terminal Myc epitope), the partial ORF was cloned into the *pTKO-CAT* plasmid at NsiI/PacI sites. The deletion variants of *Tg*CDS2, including $TgCDS2^{527-1044}$-Myc and those lacking the signal peptide ($TgCDS2_{\Delta SP}$-Myc), transit peptide ($TgCDS2_{\Delta TP}$-Myc), or the entire bipartite sequence ($TgCDS2_{\Delta BS}$-Myc) were engineered in the *pTKO-DHFR-TS* vector at NsiI/PacI sites (see primers in supplemental Table S2). The plasmid constructs were linearized with NotI and transfected into strains harboring the full-length *Tg*CDS1-HA or *Tg*CDS2-HA. To express *Tg*CDS1 and *Tg*CDS2 with dual epitopes (N-terminal Myc tag and C-terminal HA tag) as well as *Tg*PIS with a C-terminal HA tag, their cDNAs were ligated into the *pTETO7SAG1-UPKO* plasmid at NcoI/PacI sites. Constructs were linearized by NotI and then transfected into the RHΔ*ku80*-TaTi strain. Parasites expressing *Tg*PIS-HA were successively transfected with a construct encoding for *Tg*ERD2-Ty1 (regulated by p*GRA1* promoter) to do co-localization studies.

The regulatable mutant of *Tg*CDS1 (Δ*tgcds1*$_r$) was generated in two steps. First, *Tg*CDS1-HA regulated by ATc-repressible promoter (p*TETO7SAG1*) was targeted at the *TgUPRT* locus. The ORF of *Tg*CDS1 containing a C-terminal HA tag was inserted into the *pTETO7SAG1-UPKO* vector at NcoI/PacI restriction sites. The eventual construct was linearized by NotI and transfected into the RHΔ*ku80*-TaTi strain followed by negative selection for the disruption of the *TgUPRT* locus using 5-fluorodeoxyuridine (5 μM) (52). In the second step the *TgCDS1* locus was deleted by double homologous recombination in the merodiploid strain expressing an ATc-regulatable copy of *Tg*CDS1. To achieve this, the 5′- and 3′-UTRs of *TgCDS1* were amplified from the tachyzoite gDNA and cloned into the *pTKO-DHFR-TS* vector using XcmI/SpeI and HindIII/ApaI enzyme pairs, respectively. The construct was linearized using ApaI and transfected into the merodiploid strain generated in the first step. The conditional mutant was selected for the expression of DHFR-TS using 1 μM pyrimethamine (53). To make a knock-out of the *TgCDS2* gene, the 5′- and 3′-UTRs amplified from tachyzoite gDNA were cloned into the *pTUB8-CAT* plasmid at ApaI and XhoI/XbaI restriction sites, respectively. The plasmid was linearized (XbaI) and transfected into the Δ*tgcds1*$_r$ strain followed by selection for the expression of CAT using 20 μM chloramphenicol (54). The resulting strain

(Δ*tgcds1*$_r$/Δ*tgcds2*) lacked the expression of *Tg*CDS2 entirely and allowed conditional knockdown of *Tg*CDS1 by ATc.

Indirect immunofluorescence and immunoblot assays

Parasitized HFFs cultured on glass coverslips were washed with phosphate-buffered saline (PBS) 24 h post-infection, fixed with 4% paraformaldehyde for 10 min, and neutralized with 0.1 M glycine in PBS for 5 min. Cells were permeabilized with 0.2% Triton X-100 in PBS for 20 min and treated with 2% bovine serum albumin in 0.2% Triton X-100/PBS for 30 min. Samples were stained with suitable combinations of the primary antibodies (anti-HA, 1:3000; anti-Myc, 1:3000; anti-Ty1, 1:50; anti-*Tg*Fd, 1:500; anti-*Tg*F1B, 1:1000; anti-*Tg*GAP45, 1:3000; anti-*Tg*SAG1, 1:1500) for 1 h, as shown in the figures. Cells were washed 3 times with 0.2% Triton X-100 in PBS and then stained with Alexa488/594-conjugated antibodies for 45 min. After three additional washings with PBS, samples were mounted in Fluoromount G and DAPI mix (SouthernBiotech, Birmingham, AL) and stored at 4 °C. Imaging was done using a fluorescence microscope (ApoTome, Zeiss, Jena, Germany).

To perform immunoblot analysis, fresh extracellular parasites (1.5×10^7) were washed 2× with PBS, pelleted ($400 \times g$, 10 min, 4 °C), resuspended in the protein loading buffer, and subjected to denaturing gel electrophoresis. Proteins were resolved by 10% SDS-PAGE and transferred to a nitrocellulose membrane (85 mA, 90 min). The membrane was treated with 5% skimmed dry milk suspended in Tris-buffered saline and 0.2% Tween 20 (overnight, 4 °C), incubated with anti-HA (1:1,500, mouse) and anti-*Tg*HSP90 (1:1,000, rabbit) antibodies (2 h at room temperature), washed 3× for 5 min each, and then incubated with IR dyes-conjugated secondary antibodies (680RD, 800CW, each at 1:10,000 for 1 h; Li-COR Biosciences, Lincoln NE). Proteins were visualized using a Li-COR imaging system.

Lipid analysis

Parasite pellets were suspended in 0.8 ml of PBS, and lipids were extracted according to Bligh-Dyer method (55). Total lipids equivalent to 3×10^7 parasites were dried under a nitrogen gas stream and suspended in 1 ml of chloroform and methanol mixture (1:1). A 10-μl aliquot was introduced onto a Kinetex HILIC column with dimensions 50 × 4.6 mm and 2.6 μm (Phenomenex, Torrance, CA). Phospholipids were resolved at a flow rate of 1 ml/min as described before (56). The column effluent was introduced into a mass spectrometer instrument (LTQ-XL, Thermo Scientific, Waltham, MA) and analyzed by electrospray ionization in positive and negative ion modes. Calibration curves of authentic standards were used to quantify lipids. Fatty acid composition of individual lipids was determined by MS/MS. Data were processed using the package XCMS in R (R-project) (57). Only those lipid species that were reproducibly detectable in independent assays are shown in this work. Lipids that were not conclusively detectable or quantifiable, such as PtdOH, cardiolipin, DAG, and CDP-DAG, are excluded. The abbreviations reported here follow the nomenclature of the IUPAC-IUB convention.

Lytic cycle assays

Standard methods were used to determine the impact of genetic manipulation on the lytic cycle of the parasite. Tachyzoites of all strains were pretreated with or without ATc (1 μM) for 2 passages (4 days) in culture before setting up individual assays. Plaque assays were performed by infecting HFF monolayers in 6-well plates (250 parasites per well). Lipids, if supplemented, were dissolved in serum and added to plaque cultures (0.05–0.1 μM). Cultures were incubated unperturbed for 7 days in the presence or absence of ATc followed by fixation with ice-cold methanol and staining with crystal violet dye. Plaques were imaged and scored for sizes and numbers using ImageJ software (NIH, Bethesda, MD). For yield assays, 3×10^6 tachyzoites of each strain were used to infect confluent HFFs (m.o.i. 3) in the presence or absence of ATc as specified. Parasites were then syringe-released from host cells after 40 h and numerated. For replication assays, confluent HFFs cultured on coverslips in 24-well plates were infected with tachyzoites (m.o.i. 1; 40 h) and then subjected to immunostaining using anti-*Tg*GAP45 antibody, as described above. The mean percentage of vacuoles containing variable numbers of parasites was determined to examine the replication phenotype.

Virulence assays

Tachyzoites of the parental (RHΔ*ku80*-TaTi) and Δ*tgcds1*$_r$ strains were pretreated with or without ATc (1 μM) for 3 passages (6 days in cultures). ATc treatment of C57BL/6J mice (female, 6–8 weeks old) was initiated 2 days before inoculation by supplying the drug in drinking water (0.2 mg/ml) and continued for 2 weeks during infection. Animals were inoculated with fresh extracellular parasites (10^3) via an intraperitoneal route and monitored for mortality and morbidity over a period of 4 weeks. For re-infection, animals immunized with the Δ*tgcds1*$_r$ strains (ATc-treated) were challenged with tachyzoites of the parental strain (10^3) and monitored for additional 28 days.

Statistics

All data are shown as the mean with S.E. from three to six independent assays using a representative parasite clone. Statistical analyses were performed by GraphPad Prism program (v5, Prism Software Inc., La Jolla, CA). Significance was tested by analysis of variance (between different strains) or unpaired two-tailed Student's *t* test with equal variances (between treated and untreated conditions). *, $p < 0.05$; **, $p < 0.01$; ***, $p < 0.001$.

Study approval

All animal experiments were performed in strict compliance with the Animal Protection Law of the People's Republic of China (Chapter 6; Legal Protection of Laboratory Animals) and the Institutional Animal Care and Use Committee of China Agricultural University (Beijing). Assays were approved by Beijing administration committee of laboratory animals (11401300021924).

Author contributions—N. G. and P. K. conceived and designed the study. P. K. performed the experiments. C.- M. U. and D. L. M. Z. helped with the phenotype and localization assays. Q. Y. and X. S. performed the animal assays. N. G., P. K., and J. F. B. analyzed the data. X. S., J. B. H, J. F. B., and N. G. contributed reagents or analysis tools. P. K. and N. G. wrote the paper. All authors approved the manuscript.

Acknowledgments—We thank Grit Meusel (Humboldt University Berlin) for technical assistance and Jeroen W. A. Jansen (Utrecht University) for aiding the lipidomic studies.

References

1. Lyons, R. E., McLeod, R., and Roberts, C. W. (2002) *Toxoplasma gondii* tachyzoite-bradyzoite interconversion. *Trends Parasitol.* **18,** 198–201
2. Gupta, N., Zahn, M. M., Coppens, I., Joiner, K. A., and Voelker, D. R. (2005) Selective disruption of phosphatidylcholine metabolism of the intracellular parasite *Toxoplasma gondii* arrests its growth. *J. Biol. Chem.* **280,** 16345–16353
3. Welti, R., Mui, E., Sparks, A., Wernimont, S., Isaac, G., Kirisits, M., Roth, M., Roberts, C. W., Botté, C., Maréchal, E., and McLeod, R. (2007) Lipidomic analysis of *Toxoplasma gondii* reveals unusual polar lipids. *Biochemistry* **46,** 13882–13890
4. Arroyo-Olarte, R. D., Brouwers, J. F., Kuchipudi, A., Helms, J. B., Biswas, A., Dunay, I. R., Lucius, R., and Gupta, N. (2015) Phosphatidylthreonine and lipid-mediated control of parasite virulence. *PLos Biol.* **13,** e1002288
5. Gupta, N., Hartmann, A., Lucius, R., and Voelker, D. R. (2012) The obligate intracellular parasite *Toxoplasma gondii* secretes a soluble phosphatidylserine decarboxylase. *J. Biol. Chem.* **287,** 22938–22947
6. Sampels, V., Hartmann, A., Dietrich, I., Coppens, I., Sheiner, L., Striepen, B., Herrmann, A., Lucius, R., and Gupta, N. (2012) Conditional mutagenesis of a novel choline kinase demonstrates plasticity of phosphatidylcholine biogenesis and gene expression in *Toxoplasma gondii*. *J. Biol. Chem.* **287,** 16289–16299
7. Hartmann, A., Hellmund, M., Lucius, R., Voelker, D. R., and Gupta, N. (2014) Phosphatidylethanolamine synthesis in the parasite mitochondrion is required for efficient growth but dispensable for survival of *Toxoplasma gondii*. *J. Biol. Chem.* **289,** 6809–6824
8. Mazumdar, J., H. Wilson, E., Masek, K., A. Hunter, C., and Striepen, B. (2006) Apicoplast fatty acid synthesis is essential for organelle biogenesis and parasite survival in *Toxoplasma gondii*. *Proc. Natl. Acad. Sci. U.S.A.* **103,** 13192–13197
9. Ramakrishnan, S., Docampo, M. D., Macrae, J. I., Pujol, F. M., Brooks, C. F., van Dooren, G. G., Hiltunen, J. K., Kastaniotis, A. J., McConville, M. J., and Striepen, B. (2012) Apicoplast and endoplasmic reticulum cooperate in fatty acid biosynthesis in apicomplexan parasite *Toxoplasma gondii*. *J. Biol. Chem.* **287,** 4957–4971
10. Nitzsche, R., Zagoriy, V., Lucius, R., and Gupta, N. (2016) Metabolic cooperation of glucose and glutamine is essential for the lytic cycle of obligate intracellular parasite *Toxoplasma gondii*. *J. Biol. Chem.* **291,** 126–141
11. Janouskovec, J., Horák, A., Oborník, M., Lukes, J., and Keeling, P. J. (2010) A common red algal origin of the apicomplexan, dinoflagellate, and heterokont plastids. *Proc. Natl. Acad. Sci. U.S.A.* **107,** 10949–10954
12. Athenstaedt, K., and Daum, G. (1999) Phosphatidic acid, a key intermediate in lipid metabolism. *Eur. J. Biochem.* **266,** 1–16
13. Vance, J. E., and Vance, D. E. (2004) Phospholipid biosynthesis in mammalian cells. *Biochem. Cell Biol.* **82,** 113–128
14. van Dooren, G. G., and Striepen, B. (2013) The algal past and parasite present of the apicoplast. *Annu. Rev. Microbiol.* **67,** 271–289
15. Agrawal, S., van Dooren, G. G., Beatty, W. L., and Striepen, B. (2009) Genetic evidence that an endosymbiont-derived endoplasmic reticulum-associated protein degradation (ERAD) system functions in import of apicoplast proteins. *J. Biol. Chem.* **284,** 33683–33691
16. Vollmer, M., Thomsen, N., Wiek, S., and Seeber, F. (2001) Apicomplexan parasites possess distinct nuclear-encoded, but apicoplast-localized, plant-type ferredoxin-NADP+ reductase and ferredoxin. *J. Biol. Chem.* **276,** 5483–5490
17. Meissner, M., Schlüter, D., and Soldati, D. (2002) Role of *Toxoplasma gondii* myosin A in powering parasite gliding and host cell invasion. *Science* **298,** 837–840
18. Shen, H., Heacock, P. N., Clancey, C. J., and Dowhan, W. (1996) The CDS1 gene encoding CDP-diacylglycerol synthase in *Saccharomyces cerevisiae* is essential for cell growth. *J. Biol. Chem.* **271,** 789–795
19. Zhou, Y., Peisker, H., Weth, A., Baumgartner, W., Dörmann, P., and Frentzen, M. (2013) Extraplastidial cytidine diphosphate diacylglycerol synthase activity is required for vegetative development in *Arabidopsis thaliana*. *Plant J.* **75,** 867–879
20. Halford, S., Dulai, K. S., Daw, S. C., Fitzgibbon, J., and Hunt, D. M. (1998) Isolation and chromosomal localization of two human CDP-diacylglycerol synthase (CDS) genes. *Genomics* **54,** 140–144
21. Inglis-Broadgate, S. L., Ocaka, L., Banerjee, R., Gaasenbeek, M., Chapple, J. P., Cheetham, M. E., Clark, B. J., Hunt, D. M., and Halford, S. (2005) Isolation and characterization of murine Cds (CDP-diacylglycerol synthase) 1 and 2. *Gene* **356,** 19–31
22. Martin, D., Gannoun-Zaki, L., Bonnefoy, S., Eldin, P., Wengelnik, K., and Vial, H. (2000) Characterization of *Plasmodium falciparum* CDP-diacylglycerol synthase, a proteolytically cleaved enzyme. *Mol. Biochem. Parasitol.* **110,** 93–105
23. Shastri, S., Zeeman, A. M., Berry, L., Verburgh, R. J., Braun-Breton, C., Thomas, A. W., Gannoun-Zaki, L., Kocken, C. H., and Vial, H. J. (2010) *Plasmodium* CDP-DAG synthase: an atypical gene with an essential N-terminal extension. *Int. J. Parasitol.* **40,** 1257–1268
24. Lilley, A. C., Major, L., Young, S., Stark, M. J., and Smith, T. K. (2014) The essential roles of cytidine diphosphate-diacylglycerol synthase in bloodstream form *Trypanosoma brucei*. *Mol. Microbiol.* **92,** 453–470
25. D'Souza, K., Kim, Y. J., Balla, T., and Epand, R. M. (2014) Distinct properties of the two isoforms of CDP-diacylglycerol synthase. *Biochemistry* **53,** 7358–7367
26. Tamura, Y., Harada, Y., Nishikawa, S., Yamano, K., Kamiya, M., Shiota, T., Kuroda, T., Kuge, O., Sesaki, H., Imai, K., Tomii, K., and Endo, T. (2013) Tam41 is a CDP-diacylglycerol synthase required for cardiolipin biosynthesis in mitochondria. *Cell Metab.* **17,** 709–718
27. McFadden, G. I., Reith, M. E., Munholland, J., and Lang-Unnasch, N. (1996) Plastid in human parasites. *Nature* **381,** 482–482
28. Wilson, R. J., Denny, P. W., Preiser, P. R., Rangachari, K., Roberts, K., Roy, A., Whyte, A., Strath, M., Moore, D. J., Moore, P. W., and Williamson, D. H. (1996) Complete gene map of the plastid-like DNA of the malaria parasite *Plasmodium falciparum*. *J. Mol. Biol.* **261,** 155–172
29. Köhler, S., Delwiche, C. F., Denny, P. W., Tilney, L. G., Webster, P., Wilson, R. J., Palmer, J. D., and Roos, D. S. (1997) A plastid of probable green algal origin in Apicomplexan parasites. *Science* **275,** 1485–1489
30. Sheiner, L., Demerly, J. L., Poulsen, N., Beatty, W. L., Lucas, O., Behnke, M. S., White, M. W., and Striepen, B. (2011) A systematic screen to discover and analyze apicoplast proteins identifies a conserved and essential protein import factor. *PLoS Pathog.* **7,** e1002392
31. Waller, R. F., Keeling, P. J., Donald, R. G., Striepen, B., Handman, E., Lang-Unnasch, N., Cowman, A. F., Besra, G. S., Roos, D. S., and McFadden, G. I. (1998) Nuclear-encoded proteins target to the plastid in *Toxoplasma gondii* and *Plasmodium falciparum*. *Proc. Natl. Acad. Sci. U.S.A.* **95,** 12352–12357
32. Cilingir, G., Broschat, S. L., and Lau, A. O. (2012) ApicoAP: the first computational model for identifying apicoplast-targeted proteins in multiple species of Apicomplexa. *PLoS ONE* **7,** e36598
33. DeRocher, A., Gilbert, B., Feagin, J. E., and Parsons, M. (2005) Dissection of brefeldin A-sensitive and -insensitive steps in apicoplast protein targeting. *J. Cell Sci.* **118,** 565–574
34. Tonkin, C. J., Struck, N. S., Mullin, K. A., Stimmler, L. M., and McFadden, G. I. (2006) Evidence for Golgi-independent transport from the early secretory pathway to the plastid in malaria parasites. *Mol. Microbiol.* **61,** 614–630
35. Bouchut, A., Geiger, J. A., DeRocher, A. E., and Parsons, M. (2014) Vesicles bearing *Toxoplasma* apicoplast membrane proteins persist following loss of the relict plastid or Golgi body disruption. *PLoS ONE* **9,** e112096
36. Heiny, S. R., Pautz, S., Recker, M., and Przyborski, J. M. (2014) Protein traffic to the *Plasmodium falciparum* apicoplast: evidence for a sorting branch point at the Golgi. *Traffic* **15,** 1290–1304
37. Stewart, R. J., Ferguson, D. J., Whitehead, L., Bradin, C. H., Wu, H. J., and Tonkin, C. J. (2016) Phosphorylation of SNAP is required for secretory organelle biogenesis in *Toxoplasma gondii*. *Traffic* **17,** 102–116
38. Tawk, L., Dubremetz, J. F., Montcourrier, P., Chicanne, G., Merezegue, F., Richard, V., Payrastre, B., Meissner, M., Vial, H. J., Roy, C., Wengelnik, K.,

and Lebrun, M. (2011) Phosphatidylinositol 3-monophosphate is involved in *Toxoplasma* apicoplast biogenesis. *PLoS Pathog.* **7,** e1001286
39. Daher, W., Morlon-Guyot, J., Sheiner, L., Lentini, G., Berry, L., Tawk, L., Dubremetz, J. F., Wengelnik, K., Striepen, B., and Lebrun, M. (2015) Lipid kinases are essential for apicoplast homeostasis in *Toxoplasma gondii*. *Cell Microbiol.* **17,** 559–578
40. Wichroski, M. J., and Ward, G. E. (2003) Biosynthesis of glycosylphosphatidylinositol is essential to the survival of the protozoan parasite *Toxoplasma gondii*. *Eukaryot. Cell* **2,** 1132–1136
41. Debierre-Grockiego, F., and Schwarz, R. T. (2010) Immunological reactions in response to apicomplexan glycosylphosphatidylinositols. *Glycobiology* **20,** 801–811
42. Serricchio, M., and Bütikofer, P. (2012) An essential bacterial-type cardiolipin synthase mediates cardiolipin formation in a eukaryote. *Proc. Natl. Acad. Sci. U.S.A.* **109,** E954–E961
43. Serricchio, M., and Bütikofer, P. (2013) Phosphatidylglycerophosphate synthase associates with a mitochondrial inner membrane complex and is essential for growth of *Trypanosoma brucei*. *Mol. Microbiol.* **87,** 569–579
44. Amiar, S., MacRae, J. I., Callahan, D. L., Dubois, D., van Dooren, G. G., Shears, M. J., Cesbron-Delauw, M. F., Maréchal, E., McConville, M. J., McFadden, G. I., Yamaryo-Botté, Y., and Botté, C. Y. (2016) Apicoplast-localized lysophosphatidic acid precursor assembly is required for bulk phospholipid synthesis in *Toxoplasma gondii* and relies on an algal/plant-like glycerol-3-phosphate acyltransferase. *PLoS Pathog.* **12,** e1005765
45. Holthuis, J. C., and Levine, T. P. (2005) Lipid traffic: floppy drives and a superhighway. *Nat. Rev. Mol. Cell Biol.* **6,** 209–220
46. Levine, T., and Loewen, C. (2006) Inter-organelle membrane contact sites: through a glass, darkly. *Curr. Opin. Cell Biol.* **18,** 371–378
47. van Meer, G., Voelker, D. R., and Feigenson, G. W. (2008) Membrane lipids: where they are and how they behave. *Nat. Rev. Mol. Cell Biol.* **9,** 112–124
48. van Dooren, G. G., Marti, M., Tonkin, C. J., Stimmler, L. M., Cowman, A. F., and McFadden, G. I. (2005) Development of the endoplasmic reticulum, mitochondrion, and apicoplast during the asexual life cycle of *Plasmodium falciparum*. *Mol. Microbiol.* **57,** 405–419
49. Tomova, C., Humbel, B. M., Geerts, W. J., Entzeroth, R., Holthuis, J. C., and Verkleij, A. J. (2009) Membrane contact sites between apicoplast and ER in *Toxoplasma gondii* revealed by electron tomography. *Traffic* **10,** 1471–1480
50. Huynh, M. H., and Carruthers, V. B. (2009) Tagging of endogenous genes in a *Toxoplasma gondii* strain lacking Ku80. *Eukaryot. Cell* **8,** 530–539
51. Donald, R. G., Carter, D., Ullman, B., and Roos, D. S. (1996) Insertional tagging, cloning, and expression of the *Toxoplasma gondii* hypoxanthine-xanthine-guanine phosphoribosyltransferase gene. Use as a selectable marker for stable transformation. *J. Biol. Chem.* **271,** 14010–14019
52. Donald, R. G., and Roos, D. S. (1995) Insertional mutagenesis and marker rescue in a protozoan parasite: cloning of the uracil phosphoribosyltransferase locus from *Toxoplasma gondii*. *Proc. Natl. Acad. Sci. U.S.A.* **92,** 5749–5753
53. Donald, R. G., and Roos, D. S. (1993) Stable molecular transformation of *Toxoplasma gondii*: a selectable dihydrofolate reductase-thymidylate synthase marker based on drug-resistance mutations in malaria. *Proc. Natl. Acad. Sci. U.S.A.* **90,** 11703–11707
54. Kim, K., Soldati, D., and Boothroyd, J. C. (1993) Gene replacement in *Toxoplasma gondii* with chloramphenicol acetyltransferase as selectable marker. *Science* **262,** 911–914
55. Bligh, E. G., and Dyer, W. J. (1959) A rapid method of total lipid extraction and purification. *Can. J. Biochem. Physiol.* **37,** 911–917
56. Brouwers, J. F., Aalberts, M., Jansen, J. W., van Niel, G., Wauben, M. H., Stout, T. A., Helms, J. B., and Stoorvogel, W. (2013) Distinct lipid compositions of two types of human prostasomes. *Proteomics* **13,** 1660–1666
57. Smith, C. A., Want, E. J., O'Maille, G., Abagyan, R., and Siuzdak, G. (2006) XCMS: processing mass spectrometry data for metabolite profiling using nonlinear peak alignment, matching, and identification. *Anal. Chem.* **78,** 779–787

Two phylogenetically and compartmentally distinct CDP-diacylglycerol synthases cooperate for lipid biogenesis in *Toxoplasma gondii*

Pengfei Kong, Christoph-Martin Ufermann, Diana L. M. Zimmermann, Qing Yin, Xun Suo, J. Bernd Helms, Jos F. Brouwers and Nishith Gupta

J. Biol. Chem. 2017, 292:7145-7159.
doi: 10.1074/jbc.M116.765487 originally published online March 17, 2017